



The quantitative evaluation of contrast-enhanced ultrasound in the differentiation of small renal cell carcinoma subtypes and angiomyolipoma

Hui Liu^{1,2#}, Hongli Cao^{1,2#}, Lin Chen^{1,2^}, Liang Fang^{1,2}, Yingchun Liu^{1,2}, Jia Zhan^{1,2^}, Xuehong Diao^{1,2}, Yue Chen^{1,2}

¹Department of Ultrasound, Huadong Hospital, Fudan University, Shanghai, China; ²Shanghai Key Laboratory of Clinical Geriatric Medicine, Shanghai, China

Contributions: (I) Conception and design: L Chen; (II) Administrative support: L Chen, Y Chen; (III) Provision of study materials or patients: L Chen, L Fang, J Zhan, X Diao; (IV) Collection and assembly of data: H Cao, Y Liu; (V) Data analysis and interpretation: H Liu, H Cao; (VI) Manuscript writing: All authors; (VII) Final approval of manuscript: All authors.

#These authors contributed equally to this work.

Correspondence to: Lin Chen. Department of Ultrasound, Huadong Hospital, Fudan University, 221 West Yan'an Road, Shanghai 200040, China. Email: cl_point@126.com.

Background: Contrast-enhanced ultrasound (CEUS) has been widely used for renal lesion diagnosis and differential diagnosis. However, qualitative analysis of CEUS is subject to examinations with low reproducibility. This study aims to investigate the diagnostic value of CEUS quantitative parameters in differentiating small renal cell carcinoma (RCC) subtypes and angiomyolipoma (AML).

Methods: A retrospective analysis was performed on 97 cases of a small renal mass undergoing a CEUS before a radical or partial nephrectomy procedure. A region of interest (ROI) was placed in the tumor's maximum enhanced region (ROI_{max}) as much as possible, and adjacent renal cortex (ROI_{refer}) was selected from normal renal tissue around a mass of the same depth. The time-intensity curve (TIC) was used to analyze the ROI_{max} and the ROI_{refer} of the tumors quantitatively. Then the parameters of the ROI_{max} and the ROI_{refer}, including the differences between the parameters of the ROI_{max} and the ROI_{refer}, were analyzed statistically.

Results: In RCC and clear cell renal cell carcinoma (ccRCC), the peak intensity (PI), slope (SL), area under the curve (AUC), area under the wash-in curve (AWI), area under the wash-out curve (AWO), time to peak intensity (TTP) and the mean transit time (MTT) were statistically significant between ROI_{max} and ROI_{refer} (all $P=0.000$). The ΔPI ($\Delta PI = PI_{max} - PI_{refer}$), ΔSL ($\Delta SL = SL_{max} - SL_{refer}$), ΔAUC ($\Delta AUC = AUC_{max} - AUC_{refer}$), ΔAWI ($\Delta AWI = AWI_{max} - AWI_{refer}$) and ΔAWO ($\Delta AWO = AWO_{max} - AWO_{refer}$) of RCC were significantly higher than in AML ($P=0.007, 0.000, 0.003, 0.048, 0.009$, respectively), while the TTP ($\Delta TTP = TTP_{max} - TTP_{refer}$) and ΔMTT ($\Delta MTT = MTT_{max} - MTT_{refer}$) of RCC were significantly lower (both $P=0.000$). In comparison with papillary renal cell carcinoma (pRCC) and chromophobe renal cell carcinoma (chRCC), the ΔPI , ΔSL , ΔAUC and ΔAWO of ccRCC were all larger (all $P<0.05$). The sensitivity, specificity, and AUC of the combination of parameter difference for differentiating RCC from AML were 100%, 81.2%, and 0.965, respectively, and for differentiating ccRCC from pRCC and chRCC, 85.71%, 85.92% and 0.911, respectively.

Conclusions: CEUS quantitative parameters have value in differentiating small RCC from AML and

[^] ORCID: Hui Liu, 0000-0001-8872-000X; Lin Chen, 0000-0002-0237-2137; Jia Zhan, 0000-0002-2179-4095.

distinguishing ccRCC from pRCC and chRCC.

Keywords: Renal cell carcinoma (RCC); angiomyolipoma (AML); contrast-enhanced ultrasound (CEUS); quantitative analysis

Submitted Mar 05, 2021. Accepted for publication Jun 22, 2021.

doi: 10.21037/qims-21-248

View this article at: <https://dx.doi.org/10.21037/qims-21-248>

Introduction

Renal cell carcinoma (RCC) is the most prevalent primary renal malignancy that usually requires invasive treatment such as nephrectomy or partial nephrectomy and accounts for nearly 2% of all adult cancers worldwide (1). The most common subtypes are clear cell renal cell carcinoma (ccRCC), papillary renal cell carcinoma (pRCC), and chromophobe renal cell carcinoma (chRCC), comprising 70–80%, 10–15%, and 5–10% of all RCC cases, respectively (2-4). ccRCC is the most frequent, with higher rates of invasiveness and metastasis, while pRCC and chRCC are relatively rare and have better prognoses, with 5-years survival rates of 55–60%, 80–90%, and 80–100%, respectively (5,6). Angiomyolipoma (AML) is the most common benign renal neoplasm, which requires only conservative management and active surveillance. Most scholars define renal tumors with a maximum diameter <4 cm as small renal masses (7). In recent years, increasing numbers of small RCC are being detected due to advancements in modern medical imaging technology (8). Differentiating histological classification of renal tumors is of great significance to clinical treatment decision-making and prognostic evaluation. However, it is independently difficult to characterize a small RCC using conventional magnetic resonance imaging (MRI) and computed tomography (CT) due to their low temporal resolutions. Thus, B-mode ultrasound (B-mode US) should be the preferred choice for renal tumor screening, but it is limited to differentiating a small RCC from an AML (9). Fortunately, contrast-enhanced ultrasound (CEUS), a relatively new imaging technology, has the advantage of being minimally invasive, real-time, dynamic, readily accessible, and free from the radioactive and nephrotoxic properties of contrast agents. Furthermore, CEUS has a high sensitivity for avoiding false-negative cases, which saves resources without compromising effectiveness and leaves more CT or MRI availabilities for other patients in need. Thus, CEUS is more cost-effective than MRI or CT (10-12).

At present, there are more reports on CEUS qualitative analysis for oncological imaging (13), cysts (14), solid lesions (15), and pseudotumors (16). Lu *et al.* (9) found that both centripetal enhancement in the cortical phase (71.9% *vs.* 23.2%) and homogeneous peak enhancement (100% *vs.* 27.5%) were important for differentiating an AML from a ccRCC. Some researchers have reported that ccRCC is mainly characterized by heterogeneous hyperperfusion, while pRCC and chRCC mostly feature homogeneous hypoperfusion (17,18). In our more recent study, it was found that hyperenhancement (64/81, 79.0%), homogeneous enhancement (54/81, 66.7%), fast wash-out (WO) (63/81, 77.8%), and peripheral rim-like enhancement (PRE) (45/81, 55.6%) were the typical features of small RCC (19). To the extent known, some imaging findings, including enhancement intensity (hyper-, iso-, hypo-), homogeneity (homogeneous, heterogeneous), and perilesional rim-like enhancement (present, absent), are all subject to examinations with low reproducibility. Therefore, an objective quantitative analysis is of great significance to the differentiation of small RCC subtypes and AML, and CEUS quantitative parameters are of significant importance to the differentiation of small RCC subtypes and AML (6,9,20).

Some studies have reported that CEUS has value in differentiating RCC subtypes and AML (21,22), but no reports investigate its benefit in the differentiation of different small renal lesions. Thus, the present study aims to investigate the usefulness of the quantitative parameters of CEUS in the differential diagnosis of small RCC subtypes and AML.

Methods

Patient selection

The ethical committee approved this single-institution retrospective study of Huadong Hospital (No.: 20160045) with written informed consent from all patients. The

study was conducted in accordance with the Declaration of Helsinki (as revised in 2013). Between June 2015 and December 2019, 97 small renal masses in 97 consecutive patients were admitted to Huadong Hospital. Enrolled in the study were 85 RCCs (67 males and 18 females, ages ranging from 35–87 years, mean 60.5 ± 12.1 years) and 12 AMLs (5 males and 7 females, ages ranging from 37–68 years, mean 54.8 ± 8.6 years), with each patient having undergone preoperative B-mode US and CEUS. Inclusion criteria were as follows: (I) mass size less than 4 cm; (II) mass depth less than 10 cm; (III) patient having undergone CEUS before a radical or partial nephrectomy; (IV) mass pathologically confirmed the RCC or AML. Exclusion criteria were: (I) history of cardiac failure or respiratory disorders; (II) any patient having undergone invasive treatments before the CEUS; (III) incomplete video recordings of the CEUS procedure; (IV) mass was not pathologically confirmed or pathologically confirmed as another benign or malignant tumor.

Image examination

All included patients underwent B-mode US and CEUS examinations before surgery, using an ultrasound scanner (Aplio 500, Toshiba Medical Systems, Otawara, Japan) with a convex array transducer (4C1 probe, 3–5 MHz, mechanical index < 0.10). Both B-Mode US and CEUS examinations were performed by the same radiologist from our hospital (CL), who has 18 years of experience in kidney US and 14 years in kidney CEUS. B-mode US and color Doppler flow imaging (CDFI) were used to obtain the tumors' location, size, shape, margin, orientation, echogenicity, homogeneity, and blood flow signals. The B-mode US examinations obtained the optimal view presenting the renal lesions and normal surrounding adjacent parenchyma. For each patient, CEUS was performed after a B-Mode US examination, using the same scanning system. During the CEUS examination, the US contrast agent, SonoVue (Bracco, Milan, Italy), which is a sulfur hexafluoride (SF₆) microbubble stabilized by phospholipids, was shaken with 5 mL normal saline into a microbubble suspension. The amount of contrast agent ranged from 1.6–2.4 mL depending on patient height, weight, and age. A bolus of contrast agent was injected into the antecubital vein via a 20-gauge needle, followed by a 5 mL flush of 0.9% saline. A timer and video recorder were started at the same time as the contrast agent was injected. Patients were required to hold their breaths for as long

as possible, with slow, shallow breathing allowed for any patient unable to hold their breath. Real-time dynamic images were observed continuously for at least 2–3 minutes following each injection. If necessary, repeat injections were administered after the contrast dissipated. The images and video recordings of each completely recorded CUS and CEUS examination were stored on the hard disk for subsequent analysis.

Quantitative imaging analysis of CEUS

Clicking the key of time curve analysis (TCA), the quantitative analysis software equipped within Aplio 500 systems was used to analyze every complete CEUS cine-loop for each renal lesion by a different radiologist from the previous clinician and was unaware of the identities of the patients. First, a region of interest (ROI) was, as much as possible, placed in the tumor's maximum enhanced region (ROI_{max}), avoiding any surrounding renal parenchyma or large feeding vessels. Then, the adjacent renal cortex (ROI_{refer}) was selected from normal renal tissue around the mass in the same depth. In very small lesions, the ROI_{max} would cover the whole tumor. Thus, a ROI_{tumor} was used instead of a ROI_{max}. In relatively large lesions, especially in ccRCC, areas of necrosis are more likely to occur in the mass. Therefore, a ROI_{max} was used to represent a tumor's most vascularized area. The software's motion tracking technology was used to track the movement of an ROI in real-time (the error caused by tissue movement in the scanning plane can be corrected manually if necessary). We also obtained the quantitative parameters of the TIC of the ROI_{max} and the ROI_{refer}, which included: the peak intensity (PI), slope (SL), area under the curve (AUC), area under the wash-in curve (AWI), area under the wash-out curve (AWO), time to peak intensity (TTP) and mean transit time (MTT). Then we calculated subtractions of the TIC parameters between the ROI_{max} and the ROI_{refer}, including the Δ PI, Δ TTP, Δ MTT, Δ SL, Δ AUC, Δ AWI, and Δ AWO. The differences between the subtractions of the ROI_{max} and the ROI_{refer} parameters were compared among different small renal lesions.

Reference standard

Fifty-six patients underwent radical nephrectomy, and 41 patients underwent a partial nephrectomy depending to the size and location of their renal lesion. The specimens of 97 renal lesions were obtained, and histopathological examinations were performed on each.

Table 1 Patient clinical characteristics

Groups	Gender		Laterality		Tumor location			Surgical methods	
	Male	Female	Left renal	Right renal	Upper	Middle	Lower	RN	Nephron-sparing PN
AML	5 (41.7)	7 (58.3)	6 (50.0)	6 (50.0)	4 (33.3)	3 (25.0)	5 (41.7)	5 (41.7)	7 (58.3)
RCC	67 (78.8)	18 (21.2)	43 (50.6)	42 (49.4)	25 (29.4)	32 (37.6)	28 (32.9)	51 (60.0)	34 (40.0)
ccRCC	58 (81.7)	13 (18.3)	36 (50.7)	35 (49.3)	21 (29.6)	26 (36.6)	24 (33.8)	42 (59.2)	29 (40.8)
pRCC	5 (71.4)	2 (28.6)	4 (57.1)	3 (42.9)	2 (28.6)	3 (42.9)	2 (28.6)	5 (71.4)	2 (28.6)
chRCC	4 (57.1)	3 (42.9)	3 (42.9)	4 (57.1)	2 (28.6)	3 (42.9)	2 (28.6)	4 (57.1)	3 (42.9)
Comparison between groups									
RCC vs. AML									
χ^2	5.771		0.001		0.789			1.448	
P	0.016		0.970		0.674			0.229	
ccRCC vs. pRCC									
χ^2	0.024		0.000		0.121			0.052	
P	0.877		1.000		0.941			0.819	
ccRCC vs. chRCC									
χ^2	1.090		0.000		0.121			0.000	
P	0.296		1.000		0.941			1.000	
pRCC vs. chRCC									
χ^2	-		-		0.000			-	
P	1.000		1.000		1.000			1.000	

Values are presented as numbers (%). RCC, renal cell carcinoma; ccRCC, clear cell renal cell carcinoma; pRCC, papillary renal cell carcinoma; chRCC, chromophobe renal cell carcinoma; AML, angiomyolipoma; RN, radical nephrectomy; PN, partial nephrectomy.

The histopathological results for the renal lesions were used as a reference standard.

Statistical analysis

IBM SPSS software (Version 22.0, IBM Corp., Armonk, NY, USA) and MedCalc software (Version 15.2.2, Ostend, Belgium) were used for all statistical analyses, and continuous variables were expressed as mean values \pm standard deviation (SD). Discrete variables were expressed as numbers and percentages, and the differences of clinical features between RCC, AML, and RCC subtypes were analyzed using the χ^2 test. A paired sample *t*-test compared the quantitative parameters of CEUS between the ROI_{max} and the ROI_{refer}. Subtractions in CEUS quantitative parameters between the ROI_{max} and the ROI_{refer} of benign renal masses, malignant renal masses, and different RCC subtypes were examined by a normality test. Variables

following normal distribution were compared using an independent sample *t*-test, while variables not following normal distribution were compared using a Mann-Whitney U test. Finally, a receiver operating characteristic (ROC) curve of the single parameter subtraction and combined parameter subtractions between the ROI_{max} and the ROI_{refer} was drawn based on the pathological diagnosis. The sensitivity, specificity, and AUC for differentiating small RCC subtypes and AML were then obtained, with a P value <0.05 considered statistically significant.

Results

Clinical and pathological findings

In this study, pathology results were obtained following the radical (n=56) or partial nephrectomy (n=41) procedures of 97 small renal masses in 97 patients (Table 1). Of the 97

masses, 85 were RCCs (size ranging from 13–40 mm, mean size of 28.8 ± 7.1 mm), including 71 ccRCCs, 7 pRCCs, 7 chRCCs, and several AMLs (size ranging from 11–40 mm, mean size of 22.5 ± 9.7 mm). Significant differences were noted between RCC and AML in terms of gender ($P=0.016$), with males having higher RCC percentages than AML (78.8% versus 41.7%). However, there were no significant differences in location (left, right, upper, middle, lower) or surgical methods (radical or nephrectomy) among the different histological types of small renal masses ($P>0.05$).

The results of the quantitative parameters of CEUS

The quantitative parameters of the different small renal lesions between the ROI_{max} and the ROI_{refer} are shown in *Table 2*. All ROI_{max} from the different types of small renal lesions were compared with a ROI_{refer} found at the same depth. In the cases of RCC or ccRCC, the PI, SL, AUC, AWI, and AWO of the ROI_{max} were higher than those seen in the ROI_{refer} (all $P=0.000$), while the TTP and MTT of the ROI_{max} were shorter than those from the ROI_{refer} (all $P=0.000$) (*Figure 1*). In the cases of pRCC, the MTT of

Table 2 Quantitative Parameters of Different Renal Lesions

TIC parameter/t/P	RCC	ccRCC	pRCC	chRCC	AML
PI					
PI_{max} (10E-5AU)	32.84±30.26	35.81±29.71	10.14±8.85	25.41±40.84	17.33±20.31
PI_{refer} (10E-5AU)	22.70±26.99	20.65±17.79	25.26±36.50	40.93±68.77	27.65±31.65
t	3.825	6.407	-1.261	-1.359	-1.916
P	0.000	0.000	0.254	0.223	0.082
TTP					
TTP_{max} (s)	13.89±2.88	13.84±2.44	16.51±5.31	11.79±2.27	15.60±6.08
TTP_{refer} (s)	16.99±3.47	17.27±3.50	17.09±2.09	14.09±3.23	13.58±4.99
t	-7.602	-8.198	-0.240	-3.147	2.945
P	0.000	0.000	0.819	0.020	0.013
MTT					
MTT_{max} (s)	18.93±4.49	19.34±4.46	18.30±5.45	15.39±1.90	34.25±18.71
MTT_{refer} (s)	26.88±9.36	27.24±9.86	26.11±5.08	23.94±7.25	21.97±6.98
t	-8.399	-7.375	-2.791	-2.938	2.798
P	0.000	0.000	0.032	0.026	0.017
SL					
SL_{max} (10E-5AU/S)	7.71±8.15	8.48±8.46	1.91±2.28	5.67±6.26	4.22±5.75
SL_{refer} (10E-5AU/S)	4.59±4.22	4.52±4.03	3.14±3.24	6.70±6.40	7.27±9.20
t	4.679	5.294	-1.237	-0.920	-2.478
P	0.000	0.000	0.262	0.393	0.031
AUC					
AUC_{max} (10E-5AU.S)	1,340.65±1,212.73	1,458.78±1,218.74	415.26±345.68	1,067.97±1,374.97	755.11±684.43
AUC_{refer} (10E-5AU.S)	926.66±1039.24	882.88±764.02	635.31±370.44	1,662.04±2,724.01	982.15±1,007.22
t	3.993	5.578	-2.975	-1.123	-1.346
P	0.000	0.000	0.025	0.304	0.205

Table 2 (continued)

Table 2 (continued)

TIC parameter/t/P	RCC	ccRCC	pRCC	chRCC	AML
AWI					
AWI _{max} (10E-5AU.S)	157.85±153.79	166.11±151.29	76.49±99.03	155.44±213.85	71.97±62.84
AWI _{refer} (10E-5AU.S)	109.09±165.39	100.50±96.07	62.26±20.64	243.11±500.46	103.00±101.72
t	3.328	5.290	0.353	-0.773	-1.567
P	0.001	0.000	0.736	0.469	0.145
AWO					
AWO _{max} (10E-5AU.S)	1,163.62±1,088.97	1,269.70±1,102.52	338.76±252.91	912.53±1,164.46	683.05±628.93
AWO _{refer} (10E-5AU.S)	818.23±891.80	783.17±689.40	573.07±363.67	1,418.94±2,225.18	879.22±913.45
t	3.687	5.040	-3.441	-1.214	-1.286
P	0.000	0.000	0.014	0.270	0.225

Values are means ± standard deviations. RCC, renal cell carcinoma; ccRCC, clear cell renal cell carcinoma; pRCC, papillary renal cell carcinoma; chRCC, chromophobe renal cell carcinoma; AML, angiomyolipoma; PI, peak intensity; TTP, time to peak; MTT, mean transit time; SL, slope; AUC, area under the time-intensity curve; AWI, area wash-in; AWO, area wash-out; t, t value.

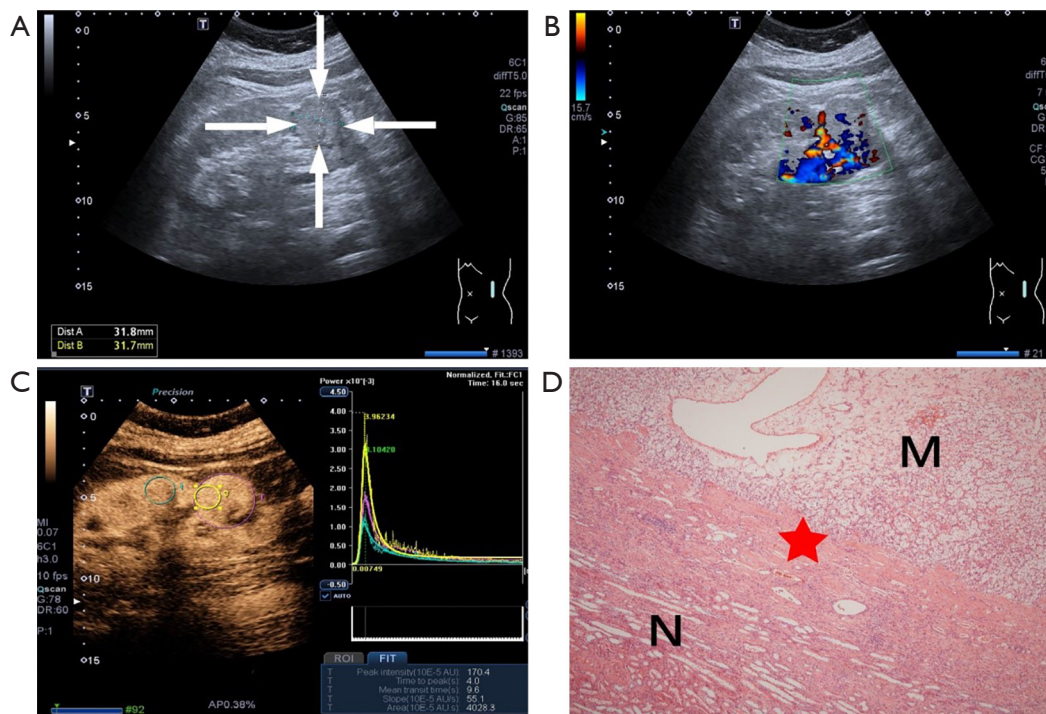


Figure 1 A 57-year-old woman with clear cell renal cell carcinoma. (A) B-Mode US showing a hypoechoic mass located in the lower pole of the left kidney (arrows); (B) color Doppler flow imaging show rich blood flow signals in and around the tumor; (C) time-intensity curve showing comparison of ROI_{refer}(green) and ROI_{tumor}(magenta). ROI_{max} (yellow) is fast wash-in, fast wash-out and hyper-enhanced; (D) photomicrograph showing the tumor pseudocapsule (asterisk) between the mass (M) and normal kidney (N). (Hematoxylin and eosin stain, ×80). ROI, region of interest.

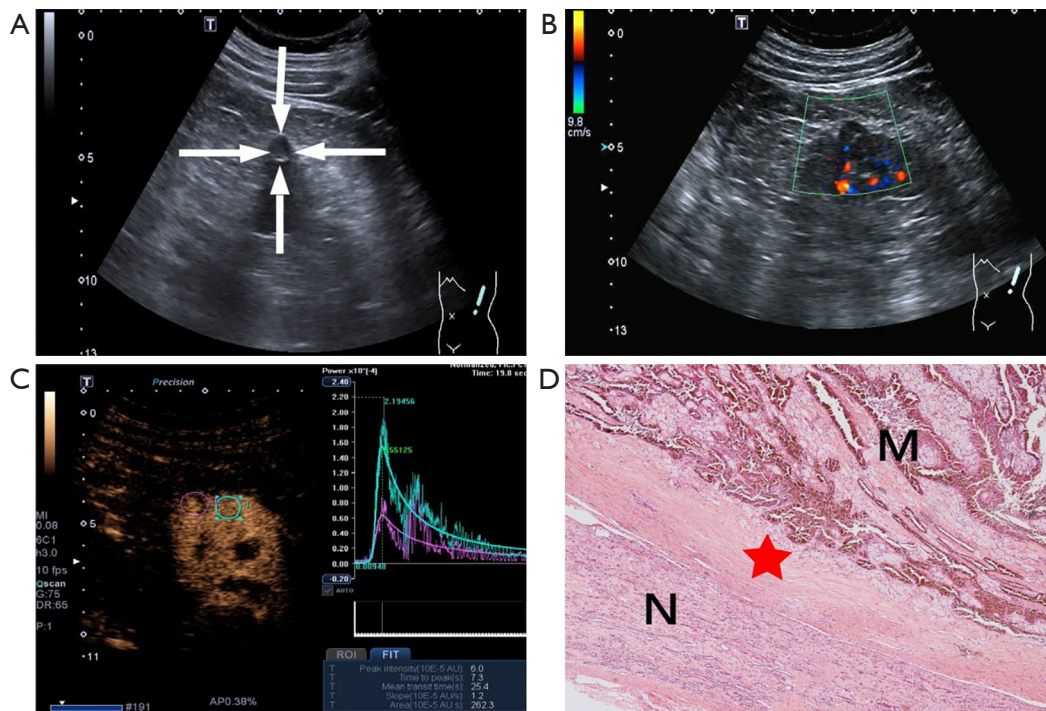


Figure 2 Forty-six-year-old man with papillary renal cell carcinoma. (A) B-Mode US showing a hypoechoic mass located in the middle of the left kidney (arrows); (B) color Doppler flow imaging show there was no blood flow signal in the tumor; (C) time-intensity curve showing comparison of ROI_{refer} (green). ROI_{tumor} (magenta) is fast wash-in, fast wash-out and hypoenhanced; (D) photomicrograph showing the tumor pseudocapsule (asterisk) between the mass (M) and normal kidney (N). (Hematoxylin and eosin stain, $\times 80$). ROI, region of interest.

the ROI_{max} was shorter than in the ROI_{refer} ($P=0.032$), and the AUC and AWO of the ROI_{max} were lower than in the ROI_{refer} ($P=0.025$, 0.014 , respectively) (Figure 2). In chRCC, the TTP and MTT of the ROI_{max} were shorter than that of the ROI_{refer} ($P=0.020$, 0.026 , respectively) (Figure 3). As for AML, the SL of the ROI_{max} was lower than seen in the ROI_{refer} ($P=0.031$), while the TTP and MTT of the ROI_{max} were longer than in the ROI_{refer} ($P=0.013$, 0.017 , respectively) (Figure 4).

The comparison of quantitative parameter subtractions between a ROI_{refer} and the ROI_{max} of different small renal lesions is shown in Table 3. The Δ PI, Δ SL, Δ AUC, Δ AWI, Δ AWO, Δ TTP, and Δ MTT differed significantly for AML and RCC (all $P<0.05$). Compared with pRCC and chRCC, in ccRCC, the Δ PI, Δ SL, Δ AUC, and Δ AWO were all larger (all $P<0.05$), while there was no statistical significance in the Δ TTP, Δ MTT, and Δ AWI. Likewise, there were no significant differences between pRCC and chRCC (all $P>0.05$).

The results show that the sensitivity, specificity, and AUC of the combination of quantitative parameter subtractions for differentiating small RCC from AML were 100%,

81.2%, and 0.965, respectively (Table 4), while the AUC of the combination of quantitative parameter subtractions for differentiating ccRCC from pRCC and chRCC was 0.911, with 85.71% sensitivity, and 85.92% specificity (Table 5).

Discussion

CEUS has unique advantages over other imaging modalities. Quantitative CEUS provides objective perfusion characteristics of renal lesions with excellent reproducibility, reducing the operator dependency of beginners by decreasing subjective errors and contributing to stable and reliable results (20,23). In our study, compared with a ROI_{refer}, the degree of RCC perfusion was higher and the contrast enhancement mode used was “fast-in and fast-out” (Figures 1–3). As for AML, the degree of perfusion was lower, and the contrast enhancement mode used was “slow-in and slow-out” (Figure 4). These characteristics were due to a correlation with the neovascularization of renal lesions. Neovascularization is closely related to tumor growth, invasion, metastasis, and recurrence (24) and is significantly

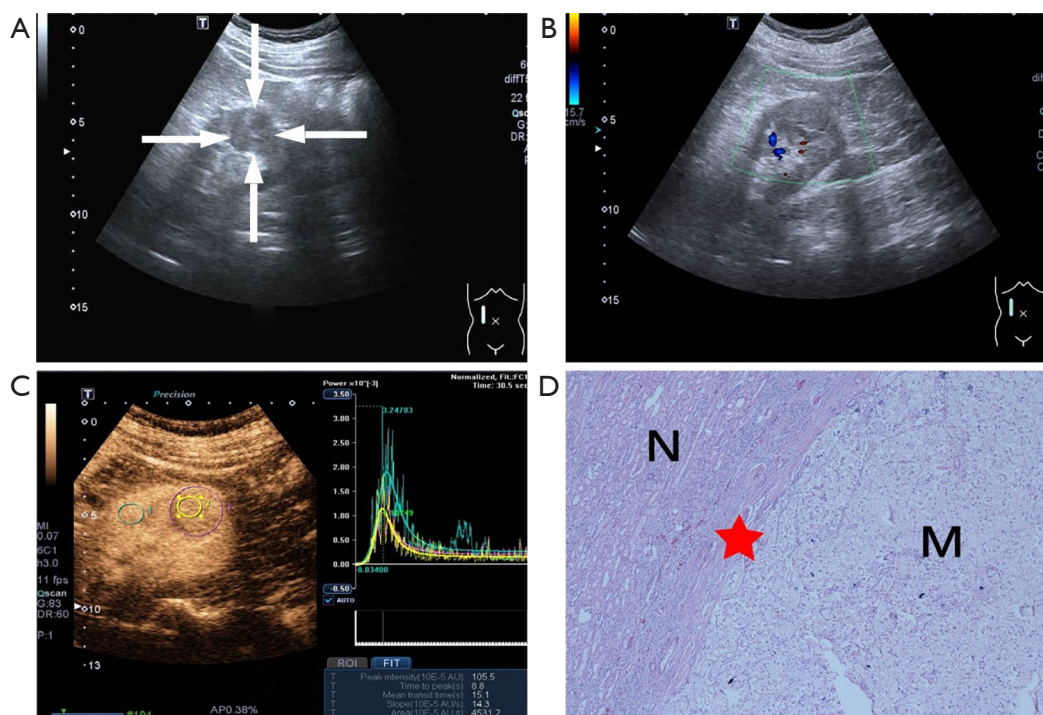


Figure 3 Sixty-two-year-old man with chromophobe renal cell carcinoma. (A) B-Mode US showing a hypoechoic mass located in the lower of the right kidney (arrows); (B) color Doppler flow imaging show there was no blood flow signal in the tumor; (C) time-intensity curve showing comparison of ROI_{refer} (green) and ROI_{tumor} (magenta). ROI_{max} (yellow) is fast wash-in, fast wash-out and hypoenhanced; (D) photomicrograph showing the tumor pseudocapsule (asterisk) between the mass (M) and normal kidney (N). (Hematoxylin and eosin stain, $\times 80$). ROI, region of interest.

different from what is seen in normal blood vessels. Blood volume is a direct marker reflecting tumor angiogenesis (25). Micro-vessel density (MVD) is the “gold standard” for the quantitative evaluation of neovascularization in tumors, but it is an invasive operation that obtains tissue specimens by surgery or puncture (26). Fortunately, TIC parameters reflect the change of ROI enhancement intensity with the time-variation after the injection of the contrast medium. Multiple parameters of blood perfusion can be extracted for quantitative analysis.

RCC is an abundant blood supply tumor with high density and thin-walled blood vessels, leading to an accelerated circulation of contrast medium and shortening perfusion and clearance. AML is characterized by malformed blood vessels, irregularly thickened walls, and narrow lumens, resulting in the slow circulation of the contrast agent and long perfusion and clearance (17,18,27). Dai *et al.* (28) demonstrated that the peak intensity of a tumor (PI) and the time to peak intensity of a tumor (TTP) between benign and malignant lesions were both statistically

significant ($P=0.003$, $P=0.000$, respectively), indicating that the perfusion of malignant lesions was higher and the time to intensity was shorter, compared with benign lesions. Our study obtained similar results to these. Sun *et al.* (6) used the $\Delta PI\%$ [$PI\% = (PI_t - PI_{refer})/PI_{refer} \times 100\%$] to correct the enhancement degree and compared the $\Delta PI\%$ of 74 malignant lesions and 19 benign lesions. The results showed a significant difference between RCC and AML in terms of $\Delta PI\%$ ($P<0.001$). Common findings of an RCC include intratumoral necrosis, hemorrhage, and calcification, which could not reflect the perfusion of tumor parenchyma. Therefore, in our study, a ROI_{max} representing the most vascularized area within the tumor has a unique advantage over a tumor’s enhanced region (ROI_{tumor}) when compared with a ROI_{refer}. Further analysis of the ROI_{tumor} among renal histotypes was not performed. We concluded that all indices (ΔPI , ΔSL , ΔAUC , ΔAWI , ΔAWO , ΔTTP , and ΔMTT) differed significantly between RCC and AML, with reliable diagnosis efficiency. The sensitivity, specificity, and AUC of the combination of parameter subtractions for

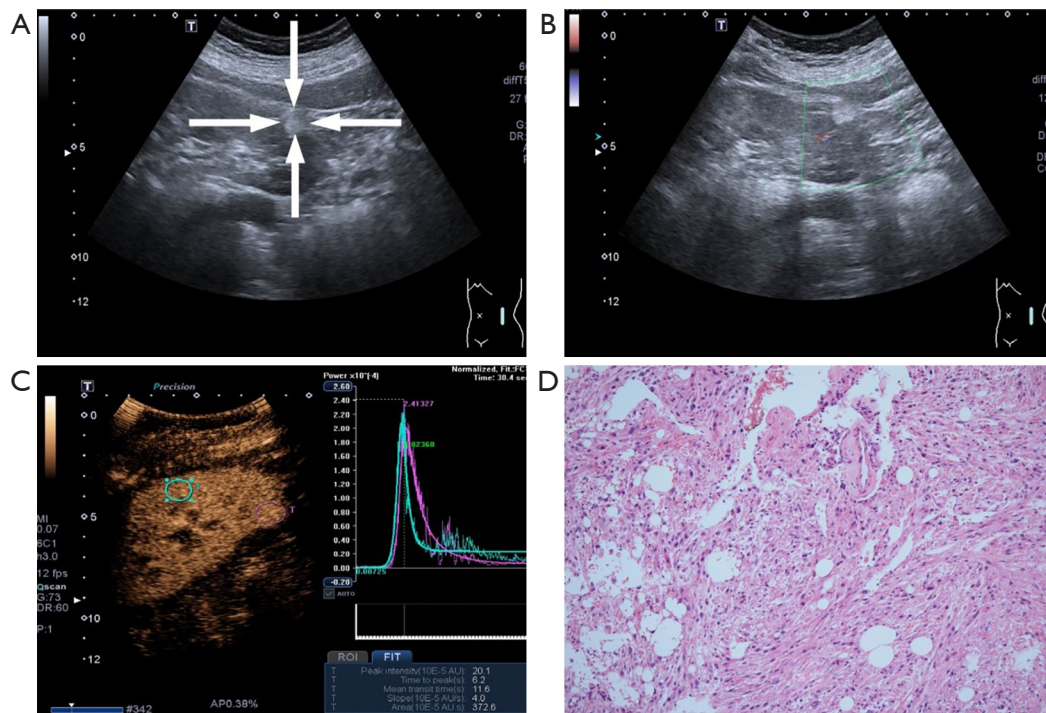


Figure 4 Sixty-five-year-old woman with renal angiomyolipoma. (A) B-Mode US showing a hyperechoic mass located in the lower of the left kidney (arrows); (B) color Doppler flow imaging showing no sign of blood flow in the tumor; (C) time-intensity curve showing comparison of ROI_{refer}(green). ROI_{tumor}(magenta) is slow wash-in, slow wash-out and hypoenhanced; (D) photomicrograph showing the tumor contained thick-walled blood vessels, smooth muscle, and fat tissue. (Hematoxylin and eosin stain, $\times 100$). ROI, region of interest.

differentiating RCC from AML were 100%, 81.2%, and 0.965, respectively (Table 4).

The incidence rate of ccRCC is the highest of the RCC subtypes, with high malignancy and a poor prognosis, while the incidence rates of pRCC and chRCC are relatively low and have lower malignancies and better prognoses. Li *et al.* (21) compared the Δ PI and Δ MTT obtained from the CEUS quantitative analysis of 341 RCCs (280 ccRCCs, 28 pRCCs, and 33 chRCCs) and 88 AMLs. The results showed that the Δ PI of the different histological types of renal tumors presents a trend of ccRCC > AML > pRCC = chRCC, and a trend of Δ MTT was AML > pRCC = chRCC = ccRCC. Similar results were obtained in our study. On this basis, we calculated the TIC parameter subtractions between the ROI_{max} and the ROI_{refer} and drew a ROC curve based on the pathological diagnosis to get the sensitivity, specificity, and AUC of the combination of parameters subtractions to diagnose RCC subtypes and AML. Lu *et al.* (22) compared the tumor-to-cortex intensity ratio (TOC-ratio) obtained by the CEUS quantitative analysis of 106 ccRCCs, 25 pRCCs, 28 chRCCs, and 34 AMLs. The results showed that pRCC

= chRCC < AML < ccRCC. Our study found that the Δ PI, Δ SL, Δ AUC, Δ and AWO of ccRCC were significantly larger than in pRCC and chRCC. The Δ TTP, Δ MTT, and Δ AWI showed no significant difference, and there was also no significant difference between pRCC and chRCC. Our study showed that the blood volume parameters of ccRCC were higher than in other RCC subtypes, while blood volume time-correlated parameters were shorter, reflecting the maximum blood volume and the highest micro-vessel density. These features were associated with ccRCC, a rich blood supply tumor with a large microvascular diameter, and distorted, interrupted, irregular, and dense blood vessels, and arteriovenous fistulas (29). pRCC and chRCC are low-grade RCC with low enhancement, with characteristics relating to pRCC being a hypovascular tumor with a small microvascular caliber and no large vessels or arteriovenous fistulas. chRCC cells show compact growth and parameters of perfusion intensity that are most consistent with those of pRCC. In this study, compared with pRCC and chRCC, the Δ TTP, Δ MTT, Δ AWI of ccRCC were not statistically significant ($P > 0.05$), potentially related to the selection

Table 3 Quantitative parameters subtractions between ROI_{max} and ROI_{refer}

Groups	Δ PI (10E-5AU)	Δ TTP (s)	Δ MTT (s)	Δ SL (10E-5AU/S)	Δ AUC (10E-5AU.S)	Δ AWI (10E-5AU.S)	Δ AWO (10E-5AU.S)
AML	-10.32±18.65	2.02±2.37	12.28±15.21	-3.05±4.26	-227.04±584.43	-31.03±68.58	-196.17±528.34
RCC	10.14±24.44	-3.10±3.76	-7.95±8.72	3.12±6.15	414.00±955.85	48.75±135.06	345.40±863.73
ccRCC	15.16±19.94	-3.43±3.53	-7.90±9.02	3.96±6.30	575.90±869.90	65.61±104.51	486.53±813.46
pRCC	-15.11±31.70	0.57±6.31	-7.81±7.41	-1.23±2.63	-220.06±195.72	14.23±106.64	-234.31±180.15
chRCC	-15.51±19.94	-2.30±1.93	-8.56±7.71	-1.03±2.96	-594.07±1,399.87	-87.67±300.22	-506.41±1,103.52
Comparison between groups							
RCC vs. AML							
t/Z	2.78	-4.575	-6.765	-4.071	-2.947	2.004	-2.630
P	0.007	0.000	0.000	0.000	0.003	0.048	0.009
ccRCC vs. pRCC							
t/Z	0.270	-1.889	-0.023	2.149	2.401	1.239	2.326
P	0.001	0.063	0.981	0.035	0.019	0.219	0.023
ccRCC vs. chRCC							
t/Z	3.70	-0.833	0.187	2.062	3.200	-1.871	2.984
P	0.000	0.408	0.852	0.043	0.002	0.061	0.004
pRCC vs. chRCC							
t/Z	-0.024	0.693	0.184	-0.134	0.700	0.846	0.644
P	0.981	0.502	0.857	0.896	0.497	0.414	0.532

Values are means ± standard deviations. RCC, renal cell carcinoma; ccRCC, clear cell renal cell carcinoma; pRCC, papillary renal cell carcinoma; chRCC, chromophobe renal cell carcinoma; AML, angiomyolipoma; PI, peak intensity; TTP, time to peak; MTT, mean transit time; SL, slope; AUC, area under the time-intensity curve; AWI, area wash-in; AWO, area wash-out.

Table 4 Diagnostic efficiency of quantitative parameter subtractions between ROI_{max} and ROI_{refer} for RCC and AML

Parameter	Cut-off value	Sensitivity	Specificity	AUC
Δ PI	1.4 (10E-5AU)	83.33%	72.94%	0.830
Δ TTP	0.1 s	91.67%	88.24%	0.942
Δ MTT	-0.7 s	91.67%	87.06%	0.947
Δ SL	-0.2 (10E-5AU/S)	91.67%	80.00%	0.864
Δ AUC	29.6 (10E-5AU.S)	75.00%	72.94%	0.764
Δ AWI	32.9 (10E-5AU.S)	100.00%	50.59%	0.768
Δ AWO	38.0 (10E-5AU.S)	75.00%	71.76%	0.735
Combination	-	100%	81.18%	0.965

RCC, renal cell carcinoma; AML, angiomyolipoma; PI, peak intensity; TTP, time to peak; MTT, mean transit time; SL, slope; AUC, area under the time-intensity curve; AWI, area wash-in; AWO, area wash-out.

Table 5 Diagnostic efficiency of quantitative parameter subtractions between ROI_{max} and ROI_{refer} for ccRCC and other types of RCC

Parameter	Cut-off value	Sensitivity	Specificity	AUC
ΔPI	-0.4 (10E-5AU)	71.43%	90.14%	0.849
ΔSL	0.2 (10E-5AU/S)	85.71%	81.69%	0.854
ΔAUC	46.6 (10E-5AU.S)	92.86%	81.69%	0.905
ΔAWO	36.4 (10E-5AU.S)	92.86%	80.28%	0.900
Combination	-	85.71%	85.92%	0.911

RCC, renal cell carcinoma; ccRCC, clear cell renal cell carcinoma; PI, peak intensity; SL, slope; AUC, area under the time-intensity curve; AWO, area wash-out.

bias of the recruited cases or similar poor vascularization. Larger ΔPI, ΔSL, ΔAUC, and ΔAWO can differentiate a ccRCC from both pRCC and chRCC with a reliable diagnosis efficiency (the area under the ROC curve was 0.849, 0.854, 0.905, and 0.900, respectively). The sensitivity, specificity, and AUC of the combination of these parameter subtractions for differentiating ccRCC from pRCC and chRCC were 85.71%, 85.92%, and 0.911, respectively.

It is worth noting that CEUS alone will not fully identify benign and malignant renal masses. For example, an AML can be expressed as high enhancement, which is difficult to identify with an RCC. Therefore, it is necessary to identify AML from RCC with hyperechogenicity in the B-Mode US and without circular perfusion in CEUS qualitative features (30). Furthermore, although it is difficult to distinguish between pRCC and chRCC by CEUS qualitative characteristics and quantitative parameters, chRCC is more likely to have a central scar, cystic changes, and necrosis than pRCC (31). Therefore, in clinical work, a combination of B-mode US, CEUS qualitative characteristics, and TIC quantitative parameters are needed to evaluate renal tumors comprehensively.

In recent research, Spiesecke *et al.* (32) indicated that a shrunken kidney, which gives the kidney and lesion a greater distance from the body's surface and smaller lesion size, may impair the image quality of CEUS examinations, while exophytic growth of a focal renal lesion results in better image quality. In our study, a "mass depth of less than 10 cm" and a "mass size of less than 4 cm" were included, and lesion sizes ranged from 11–40 mm, corresponding to a better TIC assessment. The TIC parameters can be used to study the perfusion of RCC subtypes and AML, making the results more objective (19). However, there are some limitations. First, the numbers of AML were fewer than the RCC, and the numbers of pRCC and chRCC were also fewer than the ccRCC. Therefore, prospective studies

with larger numbers of AML, pRCC, and chRCC are required to verify our results. Second, the Gain value was considerably different in our study, which may influence the intensity parameters of CEUS and represent a technical limitation. Due to individual variations such as a patient's girth and the penetration depth of renal lesions, the Gain value varied in the imaging of different lesions. Therefore, we used a Q Scan to avoid this difference to acquire the highest quality image possible. Third, in very small lesions, the ROI was placed to cover the whole tumor, but in relatively large lesions, the ROI should be placed in the highest vascularized areas as possible, avoiding areas of necrosis. These limitations may influence the assessment of tumor vascularization in general and represent a technical limitation. We performed a pathological diagnosis on all cases by radical or partial nephrectomy, but tumor microvessel density was not detected. Therefore, prospective studies are needed to verify our results. Moreover, our study did not include other benign masses (for example, oncocytoma) or other malignant (for example, metastases or lymphoma) histotypes. Further studies should be performed for the differentiation of additional renal tumor histotypes.

Conclusions

In summary, CEUS quantitative parameters can help the differentiation of small RCC and AML. Although it cannot distinguish between pRCC and chRCC, these parameters help to distinguish ccRCC, which has relatively higher malignancy, from pRCC and chRCC, which have higher ΔPI, ΔSL, ΔAUC, and ΔAWO.

Acknowledgments

Funding: This work was supported by funds from the

Shanghai Municipal Health and Family Planning Commission of China (201640285).

Footnote

Conflicts of Interest: All authors have completed the ICMJE uniform disclosure form (available at <https://dx.doi.org/10.21037/qims-21-248>). The authors have no conflicts of interest to declare.

Ethical Statement: The authors are accountable for all aspects of the work in ensuring that questions related to the accuracy or integrity of any part of the work are appropriately investigated and resolved. The study was conducted in accordance with the Declaration of Helsinki (as revised in 2013). This study was approved by the ethical committee of Huadong Hospital with written informed consent from all included patients.

Open Access Statement: This is an Open Access article distributed in accordance with the Creative Commons Attribution-NonCommercial-NoDerivs 4.0 International License (CC BY-NC-ND 4.0), which permits the non-commercial replication and distribution of the article with the strict proviso that no changes or edits are made and the original work is properly cited (including links to both the formal publication through the relevant DOI and the license). See: <https://creativecommons.org/licenses/by-nc-nd/4.0/>.

References

1. Bray F, Ferlay J, Soerjomataram I, Siegel RL, Torre LA, Jemal A. Global cancer statistics 2018: GLOBOCAN estimates of incidence and mortality worldwide for 36 cancers in 185 countries. *CA Cancer J Clin* 2018;68:394-424.
2. Kovacs G, Akhtar M, Beckwith BJ, Bugert P, Cooper CS, Delahunt B, Eble JN, Fleming S, Ljungberg B, Medeiros LJ, Moch H, Reuter VE, Ritz E, Roos G, Schmidt D, Srigley JR, Störkel S, van den Berg E, Zbar B. The Heidelberg classification of renal cell tumours. *J Pathol* 1997;183:131-3.
3. Truong LD, Shen SS. Immunohistochemical diagnosis of renal neoplasms. *Arch Pathol Lab Med* 2011;135:92-109.
4. Hagenkord JM, Gatalica Z, Jonasch E, Monzon FA. Clinical genomics of renal epithelial tumors. *Cancer Genet* 2011;204:285-97.
5. Steffens S, Roos FC, Janssen M, Becker F, Steinestel J, Abbas M, Steinestel K, Wegener G, Siemer S, Thüroff JW, Hofmann R, Stöckle M, Schrader M, Hartmann A, Junker K, Kuczyk MA, Schrader AJ; German Renal Cell Cancer Network. Clinical behavior of chromophobe renal cell carcinoma is less aggressive than that of clear cell renal cell carcinoma, independent of Fuhrman grade or tumor size. *Virchows Arch* 2014;465:439-44.
6. Sun D, Wei C, Li Y, Lu Q, Zhang W, Hu B. Contrast-Enhanced Ultrasonography with Quantitative Analysis allows Differentiation of Renal Tumor Histotypes. *Sci Rep* 2016;6:35081.
7. Sánchez-Martín FM, Millán-Rodríguez F, Urdaneta-Pignalosa G, Rubio-Briones J, Villavicencio-Mavrich H. Small renal masses: incidental diagnosis, clinical symptoms, and prognostic factors. *Adv Urol* 2008;310694.
8. Wang ZJ, Westphalen AC, Zagoria RJ. CT and MRI of small renal masses. *Br J Radiol* 2018;91:20180131.
9. Lu Q, Huang BJ, Wang WP, Li CX, Xue LY. Qualitative and quantitative analysis with contrast-enhanced ultrasonography: diagnosis value in hypoechoic renal angiomyolipoma. *Korean J Radiol* 2015;16:334-41.
10. Kazmierski B, Deurdulian C, Tehelepi H, Grant EG. Applications of contrast-enhanced ultrasound in the kidney. *Abdom Radiol (NY)* 2018;43:880-98.
11. Spiesecke P, Reinhold T, Wehrenberg Y, Werner S, Maxeiner A, Busch J, Fischer T, Hamm B, Lerchbaumer MH. Cost-effectiveness analysis of multiple imaging modalities in diagnosis and follow-up of intermediate complex cystic renal lesions. *BJU Int* 2021. [Epub ahead of print]. doi: 10.1111/bju.15353.
12. Schwarze V, Marschner C, Negrao De Figueiredo G, Ingrisich M, Rübenthaler J, Clevert DA. Single-center study: dynamic contrast-enhanced ultrasound in the diagnostic assessment of carotid body tumors. *Quant Imaging Med Surg* 2020;10:1739-47.
13. Gummadi S, Eisenbrey JR, Lyshchik A. Contrast-enhanced ultrasonography in interventional oncology. *Abdom Radiol (NY)* 2018;43:3166-75.
14. Cantisani V, Bertolotto M, Clevert DA, Correas JM, Drudi FM, Fischer T, Gilja OH, Granata A, Graumann O, Harvey CJ, Ignee A, Jenssen C, Lerchbaumer MH, Ragel M, Saftoiu A, Serra AL, Stock KF, Webb J, Sidhu PS. EFSUMB 2020 Proposal for a Contrast-Enhanced Ultrasound-Adapted Bosniak Cyst Categorization - Position Statement. *Ultraschall Med* 2021;42:154-66.
15. Stock K, Kübler H, Maurer T, Slotta-Huspenina J, Holzapfel K. CEUS-diagnosis of solid renal tumors. *Radiologe* 2018;58:553-62.
16. Spiesecke P, Fischer T, Maxeiner A, Hamm B,

- Lerchbaumer MH. Contrast-enhanced ultrasound (CEUS) reliably rules out neoplasm in developmental renal pseudotumor. *Acta Radiol* 2021;62:821-9.
17. Xue LY, Lu Q, Huang BJ, Li CX, Yan LX, Wang WP. Differentiation of subtypes of renal cell carcinoma with contrast-enhanced ultrasonography. *Clin Hemorheol Microcirc* 2016;63:361-71.
 18. Reimann R, Rübenthaler J, Hristova P, Staehler M, Reiser M, Clevert DA. Characterization of histological subtypes of clear cell renal cell carcinoma using contrast-enhanced ultrasound (CEUS). *Clin Hemorheol Microcirc* 2015;63:77-87.
 19. Chen L, Wang L, Diao X, Qian W, Fang L, Pang Y, Zhan J, Chen Y. The diagnostic value of contrast-enhanced ultrasound in differentiating small renal carcinoma and angiomyolipoma. *Biosci Trends* 2015;9:252-8.
 20. Aoki S, Hattori R, Yamamoto T, Funahashi Y, Matsukawa Y, Gotoh M, Yamada Y, Honda N. Contrast-enhanced ultrasound using a time-intensity curve for the diagnosis of renal cell carcinoma. *BJU Int* 2011;108:349-54.
 21. Li CX, Lu Q, Huang BJ, Xue LY, Yan LX, Zheng FY, Wen JX, Wang WP. Quantitative evaluation of contrast-enhanced ultrasound for differentiation of renal cell carcinoma subtypes and angiomyolipoma. *Eur J Radiol* 2016;85:795-802.
 22. Lu Q, Huang BJ, Xue LY, Fan PL, Wang WP. Differentiation of Renal Tumor Histotypes: Usefulness of Quantitative Analysis of Contrast-Enhanced Ultrasound. *AJR Am J Roentgenol* 2015;205:W335-42.
 23. Gauthier TP, Muhammad A, Wasan HS, Abel PD, Leen EL. Reproducibility of quantitative assessment of altered hepatic hemodynamics with dynamic contrast-enhanced ultrasound. *J Ultrasound Med* 2012;31:1413-20.
 24. Server S, Sabet S, Yaghouti K, Namal E, Inan N, Tokat Y. Value of Imaging Findings in the Prediction of Microvascular Invasion in Hepatocellular Carcinoma. *Transplant Proc* 2019;51:2403-7.
 25. Greis C. Quantitative evaluation of microvascular blood flow by contrast-enhanced ultrasound (CEUS). *Clin Hemorheol Microcirc* 2011;49:137-49.
 26. Mori N, Mugikura S, Takahashi S, Ito K, Takasawa C, Li L, Miyashita M, Kasajima A, Mori Y, Ishida T, Kodama T, Takase K. Quantitative Analysis of Contrast-Enhanced Ultrasound Imaging in Invasive Breast Cancer: A Novel Technique to Obtain Histopathologic Information of Microvessel Density. *Ultrasound Med Biol* 2017;43:607-14.
 27. Wei SP, Xu CL, Zhang Q, Zhang QR, Zhao YE, Huang PF, Xie YD, Zhou CS, Tian FL, Yang B. Contrast-enhanced ultrasound for differentiating benign from malignant solid small renal masses: comparison with contrast-enhanced CT. *Abdom Radiol (NY)* 2017;42:2135-45.
 28. Dai WB, Yu B, Diao XH, Cao H, Chen L, Chen Y, Zhan J. Renal Masses: Evaluation with Contrast-Enhanced Ultrasound, with a Special Focus on the Pseudocapsule Sign. *Ultrasound Med Biol* 2019;45:1924-32.
 29. Jiang J, Chen Y, Zhou Y, Zhang H. Clear cell renal cell carcinoma: contrast-enhanced ultrasound features relation to tumor size. *Eur J Radiol* 2010;73:162-7.
 30. Xu ZF, Xu HX, Xie XY, Liu GJ, Zheng YL, Lu MD. Renal cell carcinoma and renal angiomyolipoma: differential diagnosis with real-time contrast-enhanced ultrasonography. *J Ultrasound Med* 2010;29:709-17.
 31. Raman SP, Johnson PT, Allaf ME, Netto G, Fishman EK. Chromophobe renal cell carcinoma: multiphase MDCT enhancement patterns and morphologic features. *AJR Am J Roentgenol* 2013;201:1268-76.
 32. Spiesecke P, Fischer T, Friedersdorff F, Hamm B, Lerchbaumer MH. Quality Assessment of CEUS in Individuals with Small Renal Masses-Which Individual Factors Are Associated with High Image Quality? *J Clin Med* 2020;9:4081.

Cite this article as: Liu H, Cao H, Chen L, Fang L, Liu Y, Zhan J, Diao X, Chen Y. The quantitative evaluation of contrast-enhanced ultrasound in the differentiation of small renal cell carcinoma subtypes and angiomyolipoma. *Quant Imaging Med Surg* 2022;12(1):106-118. doi: 10.21037/qims-21-248